Heat Capacity Spectroscopy Compared to Other Linear Response Methods at the Dynamic Glass Transition in Poly(vinyl acetate)

M. Beiner, J. Korus, H. Lockwenz, K. Schröter, and E. Donth*

Fachbereich Physik, Universität Halle, D-06099 Halle (Saale), Germany

Received March 24, 1995; Revised Manuscript Received April 22, 1996[⊗]

ABSTRACT: Heat capacity spectroscopy measurements in the frequency range from 1.25 to 12 600 rad/s at the dynamic glass transition in poly(vinyl acetate) are reported. The data are compared to results of dielectric and shear spectroscopy in a comparable frequency range on the same sample. The peaks of the different imaginary parts do not have the same position across the main transition zone. The sequence of the peaks with increasing frequency is as follows: dielectric compliance, entropy compliance, and shear modulus. The distances between the different peaks are 0.3 ± 0.4 and 1.0 ± 0.4 frequency decades, respectively.

I. Introduction

Heat capacity spectroscopy (HCS) according to Birge and Nagel[1,2] allows the determination of the complex specific heat capacity, $c_p^*(\omega) = c_p'(\omega) - ic_p''(\omega)$, at the dynamic glass transition, α, in equilibrium.[3,4] According to the fluctuation dissipation theorem (FDT),[5] the natural frequencies of the spontaneous system fluctuations are identified with the external frequencies at which the system can absorb thermal energy.[1,6−8] HCS tests the time scale and the intensity of internal entropy fluctuations of a sample by means of the entropy response to an external temperature perturbation; in other words, $c_p^*(\omega)$ is the equilibrium entropy compliance.[9,10]

An important question is how this thermal property (or activity[10]) is related to other activities with a linear response (dielectric, shear, etc.). There are few investigations comparing frequency-dependent HCS data with data from the other activities.[6] In general, precise experiments with different linear response methods on identical samples of a glass former are rare. An analysis of the results[11−19] does not yield a consistent picture. The positions of the different loss maxima in the α relaxation zone seem to be different, whereas the shift factors are rather universal (same Vogel temperatures). These observations are in agreement with theoretical approaches (WLF scaling) assuming that different activities are sensitive to different molecular modes of the same cooperative motion at the dynamic glass transition.[9,10]

We can ask if there is a general sequence of the α traces for the different activities in the log ω vs $1/T$ diagram for all glass formers.[14] Additionally, for polymers, a comparison of frequency-dependent c_p^* data with dynamic shear data allows one to check some results of the fluctuation approach for the dynamic glass transition.[10] Polymers offer special interest because they have some internal length scales (gyration radius, entanglement spacing, characteristic length of the glass transition, Kuhn's segment length), permitting a length scaling of the results.[10]

From the experimental point of view, it is necessary to ensure a high reproducibility of the temperature measurements and a truly comparable temperature scale for the samples in the different devices and laboratorities (1 K corresponds to 0.3 frequency decades of α in an Arrhenius diagram). Similar problems are caused by the water contents of the samples in the different equipment, changing, for instance, during the measurement by drying with a gas stream originally applied for the temperature program.

As far as we know, the present experiments are the first HCS measurements on a polymer. Some experimental effort was necessary to realize the adhesion of the polymer layer to the thin (<100 nm) nickel strip of the spectrometer. In this paper, heat capacity spectroscopy data on poly(vinyl acetate) (PVAC) are compared with results from dielectric and mechanical shear spectroscopy.

II. Experimental Section

A. Samples. The poly(vinyl acetate) sample was purchased from Buna AG. The molecular weight distribution was determined by gel permeation chromatography with polystyrene standards. The molecular mass $\bar{M}_w$ is $5.6 \times 10^5 \pm 0.3 \times 10^5$ g/mol and the polydispersity $\bar{M}_w/\bar{M}_n = 3.7 \pm 0.2$. Slight branching seems to be possible. The conventional glass transition temperature T_g of our sample is 38 ± 1 °C. It was obtained by an equal-area construction from DSC measurements at a heating rate of $\dot{T} = \pm 10$ K/min using a DSC 7 from Perkin-Elmer. Absorbed moisture in poly(vinyl acetate) has a great influence on the linear response near T_g. The sample was dried under vacuum at 105 °C for 36 h before measurement. During all measurements, the samples were kept under dry nitrogen gas.

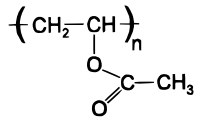

poly(vinyl acetate)

B. Measurements. The temperature−time programs in the three devices were similar. All isothermal frequency sweeps were made in the following way: After reaching the measuring temperature, the sample was annealed for 900 s. The frequency sweep was then started beginning at the lowest frequency. In the heat capacity spectrometer, the sweeps at the lowest temperature were first measured. Subsequently, the temperature was increased step by step. In the other spectrometers, the measurements were started at the highest temperatures. Practically all measurements were carried out above the conventional glass transition temperature at thermodynamic equilibrium.

1. Heat Capacity Spectroscopy (HCS). The frequency dependence of the complex product mass density × heat conductivity × heat capacity, $(\rho\kappa c_p(\omega))^*$, is measured in equi-

[⊗] Abstract published in *Advance ACS Abstracts,* June 1, 1996.

S0024-9297(95)00402-5 CCC: $12.00

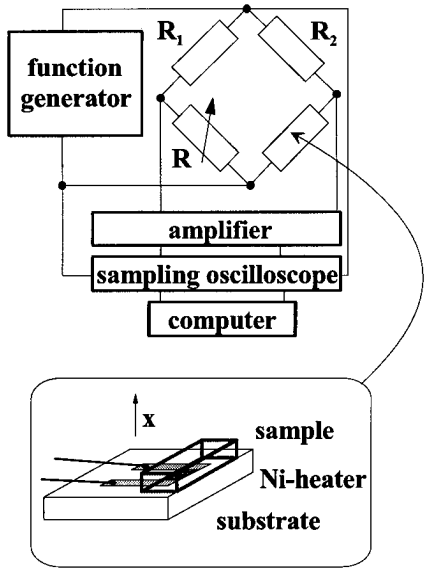

Figure 1. Experimental setup for the HCS determination of $\rho\kappa c_p^*(\omega)$ in the frequency range from 1.25 to 12 600 rad/s. The insert schematically shows the nickel heater on the surface of a substrate coated with the sample.

librium by a heat capacity spectrometer according to Birge and Nagel.[2] The experimental setup with our modifications is sketched in Figure 1. The central part of the device is a thin (70−100 nm) nickel heater on the surface of a thick (1.5 mm) substrate of glass fiber filled epoxy resin. The dimensions of the nickel strip are about 1 × 4 mm^2. The heater has a high resistance temperature coefficient (≈1000−2000 ppm·K^{-1}) and is also used as the thermometer. It was coated with the sample after a reference measurement without sample for the determination of the heater and substrate parameters. The sample thickness was 1.8 mm.

Let us recall in brief terms the main idea of HCS.[2,20] The heater is supplied with an alternating electric current $I(t) = I_0 \cos(\omega t/2)$ of frequency $\omega/2$ and amplitude I_0 during the isothermal measurements. By virtue of the high temperature coefficient of the heater resistance, the latter is modified by the diffusion of temperature waves in the surroundings (substrate and sample). The Joule dissipation, $P(t)$, in the Ni layer is

$$P(t) = I^2(t)R(t) = \frac{1}{2}R(t)I_0^2(1 + \cos(\omega t)) \tag{1}$$

where $R(t)$ is the time-dependent resistance of the heater. The periodic resistance variation of the heater, due to the temperature oscillations in the sample and substrate, is given by

$$R(t) = R_0(1 + \alpha T_\omega \cos(\omega t - \varphi)) \tag{2}$$

where R_0 is the resistance at a fixed measuring temperature, α its temperature coefficient, T_ω the temperature amplitude (typically smaller about 1 K) as a response to the alternating dissipation $P(t)$, and φ the phase shift. Ohm's law gives the voltage across the heater

$$U(t) = I(t)R(t) = R_0 I_0 \cos(\omega t/2) + \frac{1}{2}R_0 I_0 \alpha T_\omega \cos(\omega t/2 - \varphi) + \frac{1}{2}R_0 I_0 \alpha T_\omega \cos(3\omega t/2 - \varphi) \tag{3}$$

The phase-shifted part of the first and the third harmonic depends on the details of temperature diffusion in the sample and substrate. The stationary problem can be described (assuming that the heater has zero thickness and infinite area) by the one-dimensional temperature diffusion equation for the temperature oscillation in sample or substrate,

$$-i\omega\rho c_p T(x,\omega) = \kappa\frac{\partial^2 T(x,\omega)}{\partial x^2} \tag{4}$$

under the boundary condition $T(x,\omega) \to 0$ as $x \to \infty$ (for large thickness of sample and substrate), with c_p the (possibly frequency dependent) specific heat, κ the thermal conductivity, ρ the density, and x a space coordinate perpendicular to the heater area. The solution of the differential equation for an infinite half-space is

$$T(x,\omega) = T(0,\omega)e^{-k|x|} \tag{5}$$

where $T(0,\omega)$ is the complex amplitude of the temperature oscillation at the heater. The complex thermal wave vector k is

$$k = \sqrt{\frac{\omega\rho c_p}{\kappa}}e^{-i(\pi/4)} = \sqrt{\frac{\omega\rho c_p}{\kappa}}\frac{(1-i)}{\sqrt{2}} \tag{6}$$

A second boundary condition is given by Fick's first law. Let us now consider the heater between the sample and substrate. The heat flux j_q is connected to the temperature gradient at both surfaces of the heater layer, facing the sample (without index) and the substrate (index s),

$$\kappa_s\frac{\partial T}{\partial x}|_{x\to 0^-} - \kappa\frac{\partial T}{\partial x}|_{x\to 0^+} = j_q \tag{7}$$

Combining this equation with eq 5, we have[1,2,20]

$$T(0,\omega) = \frac{j_q}{\kappa k + \kappa_s k_s} = \frac{j_q e^{i(\pi/4)}}{\sqrt{\omega}(\sqrt{\rho\kappa c_p} + \sqrt{\rho_s\kappa_s c_{p_s}})} \equiv T_\omega e^{i\varphi} \tag{8}$$

Reference measurements on the unloaded system (only heater and substrate, $(\rho\kappa c_p)^* = 0$) showed that the epoxy−glass fiber substrate has no relevant relaxation in the temperature frequency region of interest; i.e., the phase shift $\varphi(T)$ is practically constant, $\pi/4$, and $(\rho_s\kappa_s c_{ps})''$ is zero. Thus, both the amplitude, $|(\rho\kappa c_p)^*|$, and phase, δ, of the complex $(\rho\kappa c_p(\omega))^*$ product for the sample can be observed from the amplitude $U_{3\omega}(\omega)$ and the phase shift $\varphi(\omega)$ of the third harmonic by

$$\sqrt{|(\rho\kappa c_p)^*|}e^{i(\delta/2)} = \frac{\alpha R_0^2 I_0^3}{2A\sqrt{\omega}U_{3\omega}}e^{i(\pi/4-\varphi)} - \sqrt{\kappa_s\rho_s c_{p_s}} \tag{9}$$

with $\rho_s\kappa_s c_{p_s}$ the product for the unloaded system taken from the reference measurement, and A the area of the heater. The real and imaginary parts of $(\rho\kappa c_p(T,\omega))^*$ can be calculated from the projections to the real and complex axes. In this way, measurements of the amplitude $U_{3\omega}$ and phase shift φ of the third harmonic across the Ni heater (eq 3) allow the calculation of the real and imaginary parts of the product $(\rho\kappa c_p)^*$ without correction terms of higher order. The only assumption is that the thermal wavelength should be small compared to the lateral dimensions of the heater and lateral and normal dimensions of the sample and substrate (thickness). Let us assume, in a first approximation, that the heat conductivity $\kappa(T,\omega)$ is constant. From now on, ρ and κ are considered as real parameters, and the complex product is written as $\rho\kappa c_p^*$. [This is usually fulfilled at the *dynamic* glass transition, $T > T_g$.[4,21] At the *thermal* glass transition (at T_g) only a bend (and not a step) of κ is observed,[22] similar to the behavior of the density. But it is the bulk modulus, i.e., the derivative of density, that shows the usual dispersion, not the density itself.] The real and imaginary parts of the heat capacity can be obtained then from the amplitude and phase shift of the third harmonic.

The determination of the third harmonic needs an experimental setup which compensates the in-phase part of the first harmonic, because the relevant amplitude $U_{3\omega}$ in the measured signal is up to 1000 times smaller than the amplitude U_ω. This was realized by a complex bridge using an on-line Fourier

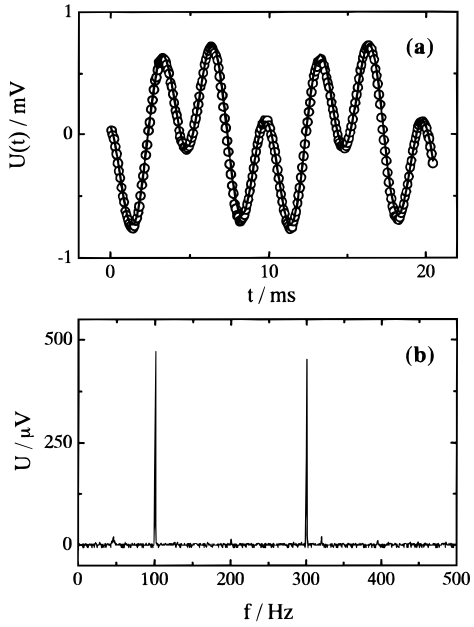

Figure 2. Output voltage from the Wheatstone bridge in the time (a) and frequency (b) domains. The solid line in part (a) is the fit by a superposition of the first and third harmonic which matches 2048 data points. For reasons of clarity, only every eighth point is shown. The frequency signal (b) is determined from 250 cycles of the time signal by a fast Fourier transformation.

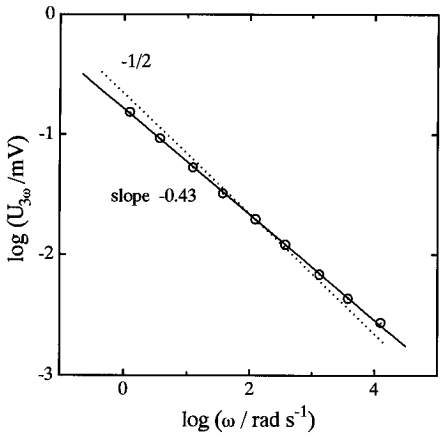

Figure 3. Frequency dependence of the amplitude $U_{3\omega}$ in the range from 1.25 to 12 600 rad/s at $T = 90$ °C. The fitted slope of −0.43 (solid line) is close to the theoretical value of −1/2 according to eq 9 (dotted line). The log symbol always means $\log_{10}$.

technique to balance the bridge. The criterion is a minimization of the amplitude ratio $U_\omega/U_{3\omega}$. The measuring signal and the stimulating signal are simultaneously detected by a DSA 602 digital oscilloscope from Tektronics (Figure 1). Figure 2a shows an example for a typical signal at 100 Hz. The amplitude and phase shift of the third harmonic are calculated externally by a fitting program using a Gauss−Jordan algorithm. It is proved that there are only sinusoidal components of the first and third harmonics of the applied frequency. This can be seen from the fast Fourier transformation (FFT) of our signal (Figure 2b) and also from the good agreement between the fit (solid line) and the experimental data (dots) in Figure 2a.

The results of frequency-dependent measurements at 90 °C in Figure 3, outside the relaxation region of the sample, demonstrate the nearly square-root dependence ($U_{3\omega} \sim \omega^{-1/2}$ in eqs 8 and 9). A linear fit in Figure 3 yields a slope of −0.43 instead of −0.50 over a broad frequency range. This effect is reproducible for the given heater. The reason for this difference is not yet clear. The actual exponent 0.43 for the frequency dependence in eq 9 was used in the data evaluation. The resulting $\rho\kappa c_p^*$ curves for the different frequencies still showed some variation in the plateau value above the transition region because small uncertainties on the logarithmic scale of Figure 3 cause a great scatter on the linear scale of $\rho\kappa c_p^*$. The values of $\rho\kappa c_p^*$ are, therefore, vertically shifted to yield the expected frequency-independent value above the dispersion region (we used a temperature of 90 °C; see Figure 4). The remaining scatter on the low-temperature side of the dynamic glass transition is probably the result of finite size effects, especially the finite width of the heater.

As the phase angle of the reference measurement differs from the theoretical value of 45° for some frequencies, in these cases its phase angle φ_0 was taken as a reference value. Usually, the deviations of the reference value φ_0 from the theoretical value 45° were smaller than 20%.

The relative error (reproducibility) of the points inside an isochronous measurement is relatively small (about the size of the symbols in Figure 4), whereas the error of the calculated absolute values for $\rho\kappa c_p'$ is considerable if all other variables (heater area A, heater resistance R_0, temperature coefficient α) are independently determined. We are trying to reduce this error by a calibration procedure.

Assuming a constant heat conductivity of $\kappa = 0.159$ W K^{-1} m^{-1} [23] and a density of $\rho = 1.191$ g cm^{-3} for PVAC, we calculated values of $c_{p_{\text{liquid}}} = 1.65 \pm 0.8$ J g^{-1} K^{-1} for the heat capacity above the dispersion zone and $\Delta c_p = c_{p_{\text{liquid}}} - c_{p_{\text{glass}}} = 0.44 \pm 0.2$ J g^{-1} K^{-1}. These values are in reasonable agreement with the results from usual nonequilibrium measurements by DSC ($c_{p_{\text{liquid}}} = 1.92$ J g^{-1} K^{-1} and $\Delta c_p = 0.48$ J g^{-1} K^{-1} [24]).

2. Dielectric and Mechanical Spectroscopy. The dielectric function $\epsilon^*(w)$ was measured in the frequency range from 0.063 to 6.3 × 10^6 rad/s (10 mHz to 1 MHz) by a commercial Novocontrol spectrometer based on a Schlumberger FRA 1260 frequency response analyzer supplemented with a high-impedance preamplifier of variable gain.[25] Additional experiments in the frequency region from 630 to 6.3 × 10^6 rad/s (100 Hz to 1 MHz) were realized by a HP4284A LCR bridge.

Measurements of the dynamic shear modulus $G^*(\omega)$ were performed in the frequency range $\omega = 0.01-100$ rad/s using a Rheometrics RDA II analyzer.

3. Comparison of Temperatures in the Different Devices. The absolute temperature displays of the three devices were checked by small resistance thermometers near the samples. These resistance thermometers are carefully calibrated in a gauge thermostat with a PT 100 having a certified accuracy of the absolute temperature scale with $\Delta T < 0.03$ K. The deviation of the absolute temperature scale was smaller than 0.3 K for the dielectric and mechanical spectrometers and is corrected for in the data evaluation. The stationary temperature difference inside the sample volume, measured with thin thermocouples, is smaller than 0.3 K for dielectric spectroscopy and smaller than 1 K for mechanical spectroscopy.[26]

In heat capacity spectroscopy, a stationary temperature difference in the sample of the order 10 K or more is caused by the time-independent part of the Joule dissipation in the heater according to eq 1. This temperature error can be corrected by a separate measurement of heater resistance with different signal amplitudes. The remaining uncertainty is smaller than 1 K. As long as the penetration depth of the temperature wave in the sample (the half thermal wavelength is 1.2 mm at $\omega = 1.25$ rad/s, the worst case) covers only a small part of the total temperature gradient, the smearing and shift of the $\rho\kappa c_p^*$ curves is expected to be small. An experimental test with a reduced power and gradient down to 25% at a frequency of 1.25 rad/s showed no difference in the $\rho\kappa c_p^*$ values larger than the experimental uncertainty of 0.5 K.

III. Results

The temperature dependence of the real part $\rho\kappa c_p'$ near the dynamic glass transition in PVAC is shown in Figure 4. The frequency-dependent dynamic glass

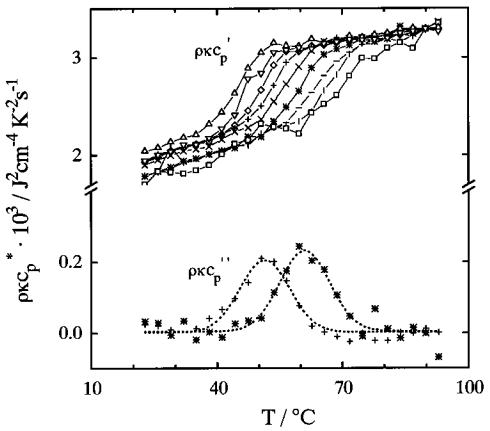

Figure 4. Temperature dependence of the real and imaginary parts of $\rho\kappa c_p^*$ (proportional to entropy compliance) for several frequencies between 1.25 and 12 600 rad/s ((△) 1.25, (▽) 3.77, (◇) 12.56, (+) 37.7, (×) 125.6, (*) 377, (—) 1256, (|) 3770, and (□) 12560 rad/s). The imaginary part is shown only for two selected frequencies. The solid lines are guides to the eye. The dotted lines are fits with a Gaussian function to the $\rho\kappa c''$ data.

transition temperature, $T_\alpha(\omega)$, shifts to higher values with increasing frequency, as expected. The $\rho\kappa c_p^*$ shift is of the order of 6 K/decade, similar to the dielectric function in the comparable frequency region (see below). Zones of $\rho\kappa c_p' = \text{const}$ are observed on the low- and high-temperature sides of the α relaxation (representing the glassy and the liquid zones, respectively). The liquid-zone real parts at 90 °C were corrected to a constant absolute value (to the measurement point at 125.6 rad/s) as described in the Experimental Section. The small variation of the glassy-zone values of the real part, below the dispersion region, is partly due to the influence of the finite heater size, the thickness of the sample and substrate, and measurement errors.

The temperature dependence of the imaginary part, $\rho\kappa c_p''$, for two selected frequencies is also illustrated in Figure 4. The results show a loss peak corresponding to the step in the real part $\rho\kappa c_p'$. The results for the imaginary part at higher frequencies, not shown here, are subject to considerable scatter because the signal-to-noise ratio dramatically decreases. For lower frequencies, the finite dimensions of the heater and sample disturb the curve shape.

The isotherms of the real part of $\rho\kappa c_p'$ as a function of logarithm of frequency are presented for several temperatures in Figure 5. The characteristic step of the dynamic glass transition was observed at all temperatures near T_g. The $\rho\kappa c_p' = \text{const}$ zones can also be detected in this representation. All isothermal representations can be approximated by the Havriliak–Negami (HN) function[27] for generalized compliances σ:

$$\Delta\sigma^*(\omega) = \sigma' - \sigma_\infty - i\sigma'' = \Delta\sigma\left[1 + \left(i\frac{\omega}{\omega_{HN}}\right)^\beta\right]^{-\gamma} \qquad (10)$$

The $\rho\kappa c_p'$ data for 56.6 °C are fitted using this HN function, which results in $\Delta(\rho\kappa c_p') = 8.3 \times 10^{-4}$ J^2 K^{-2} cm^{-4} s^{-1}, $\rho\kappa c_{p_{liquid}} = 3.1 \times 10^{-3}$ J^{2}K^{-2} cm^{-4} s^{-1}, and $\omega_{HN} = 171.4$ rad/s. The exponents are $\beta = 0.73 \pm 0.2$ and $\beta\gamma = 0.8 \pm 0.2$ with a considerable uncertainty. The curves at all other temperatures were fitted with this fixed parameter set ($\rho\kappa c_{p_{liquid}}$, $\Delta(\rho\kappa c_p')$, β, γ), because the temperature dependence of the step height Δc_p and of the shape of our equilibrium data seems to be too small to be determined with reasonable accuracy. Only the temperature dependence of ω_{HN} can be determined with reasonable confidence (see Figure 8). The fit results are satisfactory and are shown as dotted lines for the real parts in Figure 5. The imaginary part of the HN function can be calculated from the real-part fit parameters. The result is shown for 56.6 °C together with the experimental values in Figure 5. The fair coincidence demonstrates the internal consistency of the real and imaginary parts, which are independently measured. Within the experimental uncertainty, the linear response activity $\rho\kappa c_p^*(\omega)$ obeys, therefore, the Kramers–Kronig relation.[5,28]

Isothermal measurements of the dielectric permittivity $\epsilon^* = \epsilon' - i\epsilon''$ of our poly(vinyl acetate) sample in the frequency range from 0.063 to 6.3×10^6 rad/s are shown in Figure 6, a and b. The real part $\epsilon'(\omega)$ shows a steplike decrease from a higher value in the liquid state, $\epsilon_\infty + \Delta\epsilon$, to a lower value in the glassy state, ϵ_∞, similar to the heat capacity. (As well known, this behavior is characteristic for generalized compliances, in contrast to the modulus-like properties, which show an upward step.) The results are comparable with the literature data.[29] The step height, $\Delta\epsilon$, decreases with increasing temperature. The obtained $\epsilon''(\omega)$ data are fitted with a superposition of a conductivity term and a complex Havriliak–Negami function. The HN component representing the dynamic glass transition is given as a dotted line.

The results of dynamic shear measurements in the frequency range from 0.01 to 100 rad/s are presented for our sample in Figure 7. They are also similar to those of the literature.[30–32] In contrast to the other susceptibilities, for shear the modulus values, $G^*(\omega) = G'(\omega) + iG''(\omega)$, are presented, because the imaginary part of the shear compliance J'' does not show a characteristic maximum for the α relaxation (see Figure 9). The peak in J'' is hidden by the terminal transition because of the moderate molecular weight of our sample. The G' axis is logarithmically scaled because the changes of the mechanical properties at the main transition are, as a rule, dramatic in comparison to the dielectric or thermal properties (ϵ^* or c_p^*). This has some influence on the Havriliak–Negami-like fit: The experimental data are fitted only in the neighborhood of the G'' maximum. The complex MHN function (M for moduli, μ)[33] was used there,

$$\Delta\mu^* = \mu' - \mu_\infty + i\mu'' = \Delta\mu\left[1 + \left(-i\frac{\omega_{MHN}}{\omega}\right)^\beta\right]^{-\gamma} \qquad (11)$$

corresponding approximately to the HN function for compliances σ. The results are shown as dotted lines in Figure 7. There are significant deviations in the region outside the loss peak $G''(\omega)$ corresponding probably to spectral components of modified Rouse and Andrade modes. The fit is sensitive to small changes in the shape and intensity parameters, but only small changes of β, γ, and ΔG were observed.

IV. Discussion

A. Heat Capacity Spectroscopy (HCS) in the Scheme of Linear Response. In the scheme of linear response, the experimental value $\rho\kappa c_p^*$ is interpreted as a susceptibility: c_p^* is an entropy compliance related to the natural entropy fluctuation by the FDT. The experimental arguments that HCS measures the entropy compliance at the dynamic glass transition are as follows (see also ref 34):

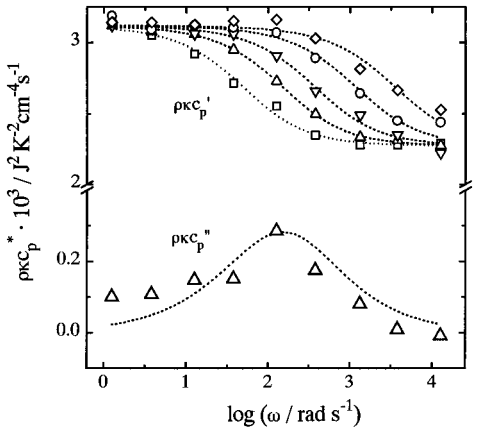

Figure 5. Isotherms for the real part of $\rho\kappa c_p'$ at the dynamic glass transition in poly(vinyl acetate) ((□) 53.6, (△) 56.6, (▽) 59.6, (○) 62.6, and (◇) 65.6 °C). The dotted lines are the results of an unbiased fit by a Havriliak−Negami function for 56.6 °C and with a partially fixed parameter set for all other temperatures (only ω_{HN} free). Also shown is the imaginary part $\rho\kappa c_p''$ at a selected temperature of 56.6 °C and the corresponding curve, calculated from the parameters of the real part fit.

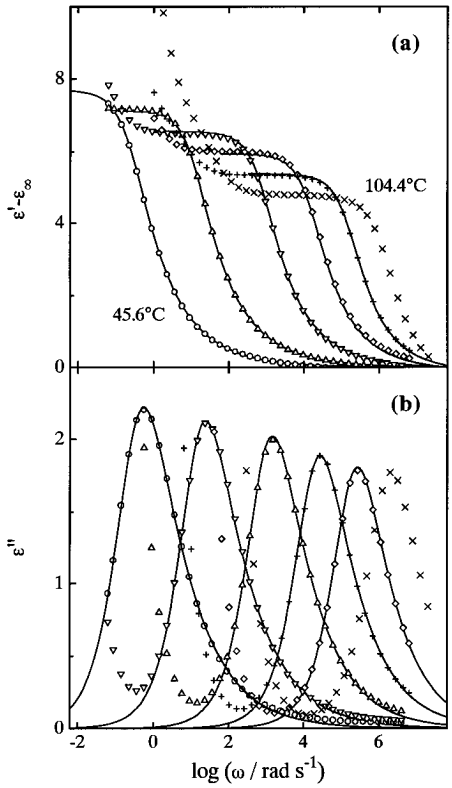

Figure 6. Frequency dependence of the real part (a) and imaginary part (b) of the dielectric function ($\epsilon^* - \epsilon_\infty$) in the frequency range from 0.063 to 6.3 × 10^6 rad/s for different temperatures ((○) 45.6, (△) 53.5, (▽) 66.5, (◇) 77.5, (+) 89.4, and (×) 104.4 °C). The data are fitted by the superposition of a complex HN function and a conductivity term. The HN component, representing the dynamic glass transition, is given by the solid lines.

(i) The frequency dependence of $\rho\kappa c_p^*$ is in accordance with the typical shape of compliances in other relaxation spectroscopy (compliance because entropy is an extensive thermodynamic variable): a step in the real part corresponds to a peak in the imaginary part, and outside the dispersion zone, the real part shows plateau values.

(ii) Consistency of $\rho\kappa c_p'$ and $\rho\kappa c_p''$ by the Kramers−Kronig relation: The shape of the real part of the entropy compliance $\rho\kappa c_p'$ in the dispersion zone can be fitted by the real part of the HN function, and, using the estimated parameters, the imaginary part can be computed in reasonable accordance with the measured values (Figure 5).

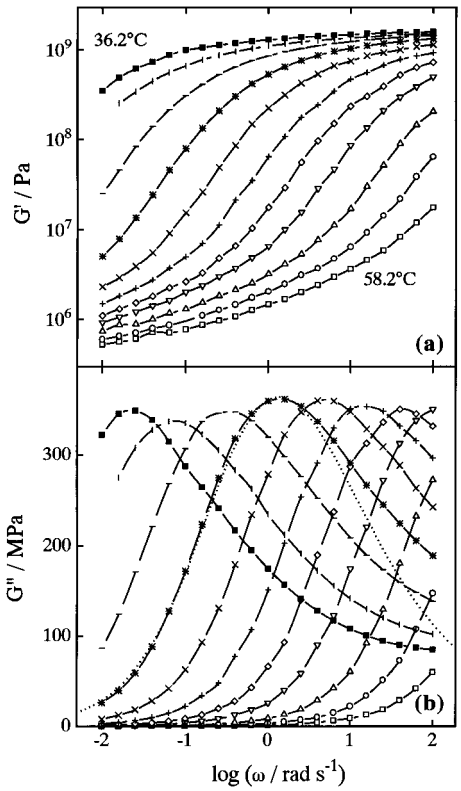

Figure 7. Isothermal frequency sweeps for the storage (a) and loss (b) parts of the shear modulus at different temperatures ((■) 36.2, (|) 37.9, (—) 39.6, (*) 41.5, (×) 43.5, (+) 45.4, (◇) 47.4, (▽) 49.4, (△) 52.3, (○) 55.2, and (□) 58.2 °C). A representative MHN fit for the loss modulus at 41.5 °C is given by the dotted line.

(iii) The equilibrium quantity $\rho\kappa c_p^*$ shows the typical properties of susceptibilities in the glass transition zone: non-Debye shape of the imaginary part, the dispersion zone moves to higher frequencies with increasing temperature, and we find a curved trace in the Arrhenius diagram (see Figure 8). The susceptibility $\rho\kappa c_p^*$ fits into the scenario of the other susceptibilities with similar VFTH parameters B and T_∞ (see Table 1).

(iv) The extrapolated $\rho\kappa c_p''$ peak temperature for a frequency of 0.01 Hz can reasonably be compared with the DSC glass transition temperature T_g.

(v) The $\rho\kappa c_p^*$ response is proportional to the disturbance temperature amplitude (linearity).

B. Comparison of Different Activities in the Glass Transition Zone. Characteristic points of the different activities are transferred to a common Arrhenius diagram (Figure 8). For HCS, the points at half step height of the real part, and for all others the maxima of imaginary parts (as calculated from spline fits), are used. (The difference between the frequencies of half step height of c_p' and maximum of c_p'' are of the order of a few percent of a decade for typical c_p^* curves. This difference is always neglected in the following discussion.) Additionally, shift factors a_T from shear measurements are also presented. The shift factors a_T were estimated by the Rheometrics software from a simultaneous horizontal shift of the G' and G'' curves (for details, see also ref 35).

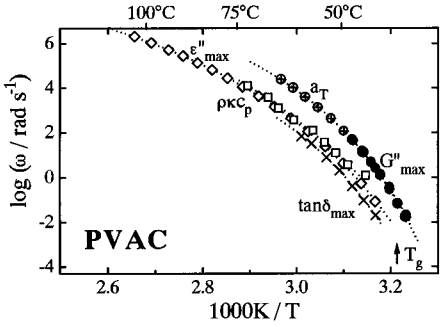

Figure 8. Common Arrhenius diagram for the α traces of the signals from different activities ((◇) ϵ''_{max}, (●) G''_{max}, (○) a_T, (■) c_p^*, (⊗) tan $\delta_{shear,max}$). The dotted lines are VFTH fits (see Table 1). The DSC glass transition temperature ($\dot{T}$ = 10 K/min) is indicated by an arrow.

Table 1. VFTH-Fit Parameters (Eq 12) for the Different Activities at the Dynamic Glass Transition of PVAC[a]

activity	T_∞/K	B	log ω_0/rad·s^{-1}
c_p^*	(251)	(990)	(14.7)
ϵ''	266 ± 3.5	660 ± 50	12.3 ± 0.3
G''	276 ± 7	450 ± 70	11.7 ± 2.2
tan δ_{mech}	277 ± 5	453 ± 100	10.1 ± 1.0
a_T	277 ± 3	420 ± 50	11.5 ± 0.3

[a] The errors are statistical uncertainties of the fit procedure. The reproducibility from repeated measurements is comparable.

The trace for the c_p^* signal fits well into the same dispersion zone as the other responses. It is curved similarly to the other susceptibilities in this frequency region. All curves seem to be only vertically shifted. With decreasing temperature, or increasing frequency, the loss peaks are sorted across the glass transition zone in the succession shear loss factor tan δ_{max}, dielectric function ϵ'', dynamic entropy compliance c_p'', and shear modulus G''. The (hidden) loss maxima for the shear compliance J'' would be at considerably lower frequencies than tan δ_{max}. The relative position of c_p'' and ϵ'' is uncertain in the limits of experimental errors.

All data sets can be approximated by the VFTH equation[36] (equivalent to the WLF equation[37]),

$$\log\left(\frac{\omega_0}{\omega}\right) = \frac{B}{T - T_\infty} \qquad (12)$$

where B, ω_0, and T_∞ are the fitting parameters. Polymers usually show VFTH behavior over a wide frequency range (10^{-2}–10^9 rad/s). The VFTH curves for the dielectric loss maxima, the maxima in G'', the shift factors a_T, and the mechanical loss tangent are given as dotted lines in Figure 8. The VFTH fit parameters are listed in Table 1. The parameters for the c_p^* data are, of course, more uncertain than the others. The estimated parameters for T_∞ compare well with literature results of 271 K from dielectric measurements[29] and 279 K from shear.[32]

The imaginary parts of the shear modulus and the compliances from the different activities at 56.6 °C are compared in Figure 9. Considerable differences in the position of different activities are observed (similarly to Figure 8, of course). The distance between the loss maxima of ϵ'' and G'' is 1.3 ± 0.3 frequency decades, equivalent to about 5 K. This is beyond the experimental uncertainty of the temperatures. The distance between c_p'' and ϵ'' amounts to only 0.3 ± 0.4 frequency decades, so that no clear decision can be made. The width of the peaks is also different. Whereas c_p'' and ϵ'' are rather sharp (about 2 frequency decades), the peak

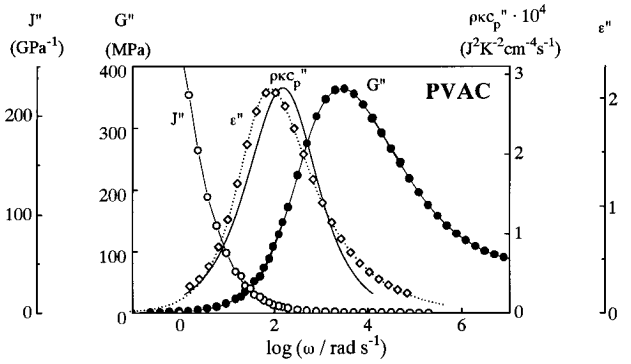

Figure 9. Loss peaks for the different activities at a reference temperature of 56.6 °C. The solid line is for dynamic entropy compliance calculated from the parameters of the real part fit. The dielectric function (◇) and the master curves for shear compliance (○) and shear modulus (●) were slightly VFTH shifted from temperature-neighbored experiments to the same reference temperature.

in G'' is broader (about 3 frequency decades). The shear compliance curve in Figure 9 shows that the J'' loss peak at the dynamic glass transition is superposed by the high-frequency wing of the flow transition but also that the α peak maximum lies at significantly lower frequencies as for the other activities.

We interpret Figure 9 in the following way:[10] Generally, any compliance emphasizes longer times than the conjugate modulus. Moreover, each experimental method (we have different properties or activities[10]) is specifically sensitive to the general, broad frequency spectrum of the cooperative motions at the dynamic glass transition (or main transition). The dielectric detection is based, for example, on changes of the dipole moments, while specific heat spectroscopy feels only entropy-active motions changing the molecular disorder. Shear response is rather sensitive to all modes.

From this point of view, it is expected that there are differences in the temperature−frequency position and shape of the α loss peaks from different susceptibilities. Assuming a common dispersion law for the cooperative motions,[10] we can see from Figure 9 that the G'' peak is sensitive to shorter modes, whereas the ϵ'' and c_p'' peaks are sensitive to longer modes of the cooperativity.

V. Conclusion

The dynamic entropy compliance c_p^* behaves similarly to the dielectric compliance ϵ^* at the dynamic glass transition in poly(vinyl acetate). The frequency sweeps can be fitted by a HN function and the α traces in an Arrhenius diagram are similarly curved. The investigated activities $c_p^*(\omega)$, $\epsilon^*(\omega)$, and $G^*(\omega)$ in poly(vinyl acetate), under isothermal conditions, have different frequency positions of the loss peaks; the difference between c_p'' and G'' is about one decade. The dynamic entropy compliance peak probably has slightly higher frequencies than the dielectric function.

Acknowledgment. The authors are grateful to the Deutsche Forschungsgemeinschaft for financial support of this work.

References and Notes

(1) Birge, N. O. *Phys. Rev. B* **1986**, *34*, 1631.
(2) Birge, N. O.; Nagel, S. R. *Rev. Sci. Instrum.* **1987**, *58*, 1464.
(3) Birge, N. O.; Nagel, S. R. *Phys. Rev. Lett.* **1985**, *54*, 2674.
(4) Dixon, P. K.; Nagel, S. R. *Phys. Rev. Lett.* **1988**, *61*, 341.
(5) Landau, L. D.; Lifschitz, E. M. *Lehrbuch der theoretischen Physik, Bd. V*; Akademie-Verlag: Berlin, 1987.

(6) Birge, N. O.; Jeong, Y. H.; Nagel, S. R. *Ann. N.Y. Acad. Sci.* **1986**, *484*, 101.
(7) Wunderlich, B.; Jin, Y.; Boller, A. *Thermochim. Acta* **1994**, *238*, 277.
(8) Hodge, I. M. *J. Non-Cryst. Solids* **1994**, *169*, 211.
(9) Donth, E. *Glasübergang*; Akademie-Verlag: Berlin, 1981.
(10) Donth, E. *Relaxation and Thermodynamics in Polymers. Glass Transition*; Akademie-Verlag: Berlin, 1992.
(11) Colmenero, J.; Alegria, A.; Santangelo, P. G.; Ngai, K. L.; Roland, C. M. *Macromolecules* **1994**, *27*, 407.
(12) Ferry, J. D.; Fitzgerald, E. R. *J. Colloid Sci.* **1953**, *8*, 224.
(13) Ferry, J. D.; Strella, S. *J. Colloid Sci.* **1958**, *13*, 459.
(14) Donth, E.; Schenk, W.; Ebert, A. *Acta Polym.* **1979**, *30*, 540. Donth, E.; Schneider, K. *Acta Polym.* **1985**, *36*, 273. Schneider, K.; Donth, E. *Acta Polym.* **1986**, *37*, 333. Schneider, K. Thesis, TH Leuna-Merseburg, 1984.
(15) Colmenero, J.; Alegria, A.; Alberdi, J. M.; Alvarez, F.; Frick, B. *Phys. Rev. B* **1991**, *44*, 7321.
(16) Boese, D.; Momper, B.; Meier, G.; Kremer, F.; Hagenah, J.-U.; Fischer, E. W. *Macromolecules* **1989**, *22*, 4416.
(17) Böhmer, R.; Sanchez, E.; Angell, C. A. *J. Phys. Chem.* **1992**, *96*, 9089.
(18) Garwe, F.; Schönhals, A.; Beiner, M.; Schröter, K.; Donth, E. *J. Phys.: Condens. Matter* **1994**, *6*, 6941. Beiner, M.; Garwe, F.; Hempel, E.; Schawe, J.; Schröter, K.; Schönhals, A.; Donth, E. *Physica A* **1993**, *201*, 72.
(19) Alig, I.; Stieber, F.; Wartewig, S.; Fytas, G. *Polymer* **1988**, *29*, 975.
(20) Bae, D. J.; Lee, K. B.; Jeong, Y. H.; Lee, S. M.; Kwun, S. I. *J. Korean Phys. Soc.* **1993**, *26*, 137.
(21) Sandberg, O.; Bäckström, G. *J. Polym. Sci., Polym. Phys. Ed.* **1980**, *18*, 2123.
(22) Barker, R. E.; Chen, R. Y. S.; Frost, R. S. *J. Polym. Sci., Polym. Phys. Ed.* **1977**, *15*, 1199.
(23) *Concise Encyclopedia of Polymer Science and Engineering*; Kroschwitz, J. I., Ed.; Wiley & Sons: New York, 1990; p V/72.
(24) Korus, J.; Hempel, E.; et al. (Comparison of DSC and heat capacity spectroscopy), to be published.
(25) Kremer, F.; Boese, D.; Meier, G.; Fischer, E. W. *Prog. Colloid Polym. Sci.* **1989**, *80*, 129.
(26) Bierbach, T. Diploma thesis, Universität Halle, 1995.
(27) Havriliak, S.; Negami, S. *J. Polym. Sci., Part C: Polym. Symp.* **1966**, *14*, 99.
(28) Schwarzl, F. R.; Struik, L. C. E. *Adv. Mol. Relax. Processes* **1967−1968**, *1*, 201.
(29) Schlosser, E.; Schönhals, A. *Polymer* **1991**, *32*, 2135.
(30) Williams, M. L.; Ferry, J. D. *J. Colloid Sci.* **1954**, *9*, 479.
(31) Kovacs, A. J.; Stratton, R. A.; Ferry, J. D. *J. Phys. Chem.* **1963**, *67*, 152.
(32) Plazek, D. J. *Polym. J.* **1980**, *12*, 43.
(33) Schlosser, E.; Schönhals, A.; Carius, H.-E.; Goering, H. *Macromolecules* **1993**, *26*, 6027.
(34) Nagel, S. R. In *NATO ASI Lectures*; Riste, T., Sherrington, D., Eds.; Geilo, Norway, 1993.
(35) Reissig, S.; Beiner, M.; Vieweg, S.; Schröter, K.; Donth, E. *Macromolecules*, in press.
(36) Vogel, H. *Z. Phys.* **1921**, *22*, 645. Fulcher, G. S. *J. Am. Ceram. Soc.* **1925**, *8*, 339. Tamman, G.; Hesse, W. *Z. Anorg. Allg. Chem.* **1926**, *156*, 245.
(37) Williams, M. L.; Landel, R. F.; Ferry, J. D. *J. Am. Chem. Soc.* **1955**, *77*, 3701.

MA9504025